Microwave transitions of pairs of cold Rb Rydberg atoms as Forster resonances of Floquet states

Jeonghun Lee,* Javed Iqbal,† and T. F. Gallagher
Department of Physics, University of Virginia, Charlottesville, Virginia 22904-0714, USA
(Received 19 March 2017; published 10 July 2017)

Previous measurements of single photon $nd_{5/2}nd_{5/2} \rightarrow (n+1)d_j(n-2)f$ transitions by two of us were described as microwave transitions made possible by configuration interaction (CI) between the $nd_{5/2}nd_{5/2}$ and the nearly degenerate $(n+2)p_{3/2}(n-2)f$ states [Lee and Gallagher, Phys. Rev. A **93**, 062509 (2016)]. Here we report the observation of the one photon $nd_{5/2}nd_{5/2} \rightarrow (n+3)s_{1/2}(n-2)f$, two photon $nd_{5/2}nd_{5/2} \rightarrow (n+3)p_j(n-2)f$, and three photon $nd_{5/2}nd_{5/2} \rightarrow (n+4)s_{1/2}(n-2)f$ microwave transitions. We show that both single and multiphoton microwave transitions are conveniently described as Forster resonant energy transfers between resonant Floquet states, and we show that the Floquet-Forster model reduces to the CI model used previously. Finally, to show that the transitions observed previously are by no means unique, we report pair transitions with different initial and final states as well as radio instead of microwave frequencies.

DOI: 10.1103/PhysRevA.96.012507

I. INTRODUCTION

Microwave fields provide a convenient way to probe and control Rydberg atoms and their interactions, as shown by a few examples. The observation of the motion of Rb Rydberg atoms on a repulsive van der Waals potential has been observed by Teixeira *et al.* [1] who followed the changing frequency shift of a microwave transition. Microwaves and radio frequency fields have been used to control Forster resonant energy transfer, recently in cold Rydberg atom samples by van Ditzhuizen *et al.* [2], and some time ago in samples of room temperature atoms by Pillet *et al.* [3]. Microwaves have also been used to select pairs of atoms with well-defined dipole–dipole interactions [4]. There are several recent reports of transitions of pairs of Rydberg atoms [5–7]. Of particular relevance to the present work, we reported the microwave spectroscopy of pairs of Rb Rydberg atoms. In particular, we observed transitions in which a pair of Rb $nd_{5/2}$ atoms, in the $nd_{5/2}nd_{5/2}$ molecular state, absorbed a single microwave photon and underwent the transition to the $(n+1)d_j(n-2)f$ state. In spite of the fact that only one photon was absorbed, both atoms changed state. We described the process in terms of a configuration interaction (CI) model, in which the dipole–dipole interaction induced admixture of the energetically nearby $(n+2)p_{3/2}(n-2)f$ state into the $nd_{5/2}nd_{5/2}$ state allows the microwave transition to the $(n+1)d_j(n-2)f$ state.

Here we describe the extension of the observations to multiphoton transitions between pairs of atoms. Specifically, we have observed the one photon $nd_{5/2}nd_{5/2} \rightarrow (n+3)s_{1/2}(n-2)f$, two photon $nd_{5/2}nd_{5/2} \rightarrow (n+3)p_j(n-2)f$, and three photon $nd_{5/2}nd_{5/2} \rightarrow (n+4)s_{1/2}(n-2)f$ microwave transitions. All of these processes can be described in terms of Forster resonant dipole–dipole energy transfers between Floquet, or microwave dressed, states. In this approach we treat the interaction of the atoms with the microwave field first, and then the dipole–dipole interaction between the resulting Floquet states. This approach is similar to that followed by van Ditzhuizen *et al.* [2] and Pillet *et al.* [3], but it differs in that the microwave field interacts with only one of the two atoms of the pair; the other is simply a spectator. The spectator atom is analogous to the spectator Rydberg electron in isolated core excitation of two electron Rydberg atoms [8,9]. The Floquet approach provides a convenient way to treat multiphoton processes, and it reduces to the CI model for single photon transitions. Finally, to show the generality of these transitions we describe transitions involving different initial and final states.

In the sections which follow we present the Floquet model, describe the experimental approach, present our experimental observations and compare them to the expectations from the model.

II. FLOQUET MODEL OF FORSTER ENERGY TRANSFER

In Fig. 1 we show one, two, and three photon microwave transitions from $nd_{5/2}nd_{5/2}$ pairs to other states of the form $n's_{1/2}(n-2)f$ and $(n+3)p_j(n-2)f$. Previously we described one photon transitions using a CI model, in which the dipole–dipole interaction of the $nd_{5/2}nd_{5/2}$ state with the nearby $(n+2)p_{3/2}(n-2)f$ state admixes some of the latter into the nominal $nd_{5/2}nd_{5/2}$ state. With this admixture a relatively weak microwave field can drive the $nd_{5/2}nd_{5/2}$ to $(n+3)s_{1/2}(n-2)f$ transition. In the case of the two and three photon transitions, a stronger microwave field is required, and except for the most closely spaced pairs, the interaction with the microwave field is much stronger than the dipole–dipole interaction. Accordingly, our approach is to treat the interaction of the atoms with the microwave field first, using a Floquet approach and ignoring the dipole–dipole interaction, and then introduce the dipole–dipole interaction between the resulting Floquet states. When the microwave frequency brings Floquet states into degeneracy, Forster resonant energy transfer occurs due to the dipole–dipole interaction. For the case in which a single microwave photon is absorbed or emitted the Floquet approach reduces to the result given by the CI approach used previously [5,6].

For concreteness we consider the system shown in Fig. 1, specifically the one, two, and three microwave photon

*jl7rf@virginia.edu
†Present address: Department of Physics, University of Azad and Kashmir, Muzaffarabad 13100, AJK, Pakistan.

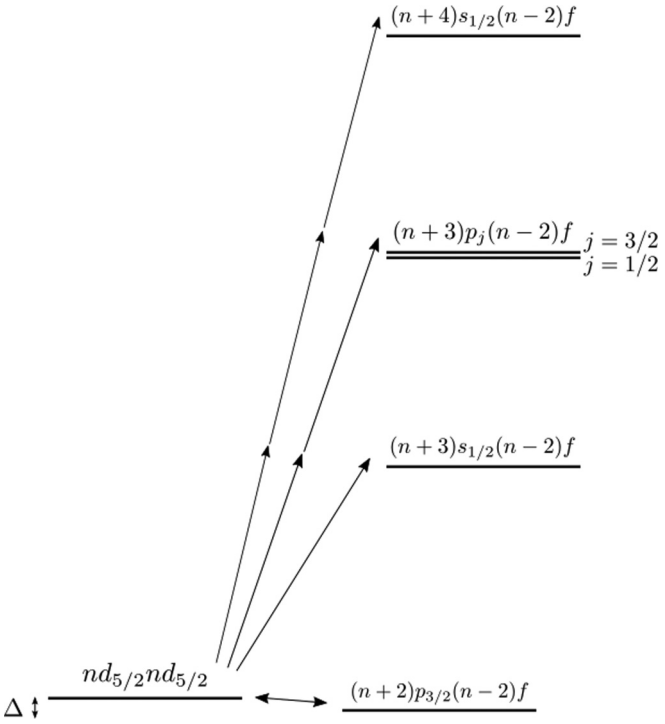

FIG. 1. One-, two-, and three-photon microwave transitions from the $nd_{5/2}nd_{5/2}$ state. The transitions to $(n+3)p_j(n-2)f$ states are two-photon transitions, and the transition to the $(n+4)s_{1/2}(n-2)f$ state is a three-photon transition. The diagram is approximately to scale.

transitions:

$$nd_{5/2}nd_{5/2}+\hbar\omega \rightarrow (n+3)s_{1/2}(n-2)f, \tag{1a}$$
$$nd_{5/2}nd_{5/2}+2\hbar\omega \rightarrow (n+3)p_{1/2}(n-2)f, \tag{1b}$$
$$nd_{5/2}nd_{5/2}+2\hbar\omega \rightarrow (n+3)p_{3/2}(n-2)f, \tag{1c}$$
$$nd_{5/2}nd_{5/2}+3\hbar\omega \rightarrow (n+4)s_{1/2}(n-2)f. \tag{1d}$$

All of these transitions are allowed due to the dipole–dipole interaction of the $nd_{5/2}nd_{5/2}$ state with the nearby $(n+2)p_{3/2}(n-2)f$ state, as shown by the double-headed arrow in Fig. 1. We ignore the $(n+2)p_{1/2}(n-2)f$ state since it is not coupled to the $nd_{5/2}nd_{5/2}$ state by the dipole–dipole interaction, and its inclusion does not significantly affect the Floquet levels at the resonant frequencies.

Unless stated otherwise we use atomic units, and for compactness in notation we introduce the shorthand,

$$\begin{aligned} nd_{5/2} &\rightarrow d,\\ (n+2)p_{3/2} &\rightarrow p,\\ (n+3)s_{1/2} &\rightarrow s,\\ (n+3)p_{1/2} &\rightarrow p_1',\\ (n+3)p_{3/2} &\rightarrow p_3',\\ (n+4)s_{1/2} &\rightarrow s',\\ (n-2)f &\rightarrow f. \end{aligned} \tag{2}$$

With this notation the transition of Eq. (1a) is written as $dd+\hbar\omega \rightarrow sf$.

The wave functions for the molecular states are direct products of the two atomic wave functions, and we ignore exchange. The energies of the molecular states at $R=\infty$, where R is the distance between the two atoms, are obtained by adding the energies of the two atomic states, which are easily calculated using the known Rb quantum defects [10–12].

The molecular dipole matrix elements which are important for the microwave coupling are

$$\begin{aligned} \langle pf|\mu|sf\rangle &= \langle p|\mu|s\rangle\langle f||f\rangle = \langle p|\mu|s\rangle = \mu_{ps},\\ \langle sf|\mu|p_1'f\rangle &= \langle s|\mu|p_1'\rangle\langle f||f\rangle = \langle s|\mu|p_1'\rangle = \mu_{sp_1'},\\ \langle sf|\mu|p_3'f\rangle &= \langle s|\mu|p_3'\rangle\langle f||f\rangle = \langle s|\mu|p_3'\rangle = \mu_{sp_3'},\\ \langle p_1'f|\mu|s'f\rangle &= \langle p_1'|\mu|s'\rangle\langle f||f\rangle = \langle p_1'|\mu|s'\rangle = \mu_{p_1's'},\\ \langle p_3'f|\mu|s'f\rangle &= \langle p_3'|\mu|s'\rangle\langle f||f\rangle = \langle p_3'|\mu|s'\rangle = \mu_{p_3's'}. \end{aligned} \tag{3}$$

In each of these transitions one atom undergoes the transition while the other remains a spectator in the $(n-2)f$ state. These molecular matrix elements are reminiscent of isolated core excitation of the two-electron Rydberg atoms [8,9]. The frequencies relevant to the transitions shown in Fig. 1 are not near any atomic frequencies for either the atomic f or d states. For this reason the $(n-2)f$ atom is simply a spectator in the microwave transitions, and an nd atom is unaffected by the microwave field.

The dipole–dipole interaction which is important for all transitions shown in Fig. 1 is

$$V_{dd} = \langle nd_{5/2}nd_{5/2}|\frac{\mu\mu'}{R^3}|(n+2)p_{3/2}(n-2)f\rangle, \tag{4}$$

where μ and μ' are the dipole matrix elements of the two atoms. It can be written as

$$\begin{aligned} V_{dd} &= \frac{\langle nd_{5/2}|\mu|(n+2)p_{3/2}\rangle\langle nd_{5/2}|\mu'|(n-2)f\rangle}{R^3}\\ &= \frac{\mu_{dp}\mu_{df}}{R^3}. \end{aligned} \tag{5}$$

Before we begin the description of the Floquet model for the transitions shown in Fig. 1, it is useful to summarize the CI model for the single photon $dd \rightarrow sf$ transition. Specifically, we are interested in calculating the fractional population transfer (FPT) from the dd to the sf state at resonance. To calculate it we calculate the transition probability for a pair of atoms spaced by R and then average over the spacings in the trap volume, as explained in some detail elsewhere [5].

Due to the dipole–dipole interaction the dd state excited by the laser has a small admixture of the pf state, so that at any finite separation R the state $|dd_R\rangle$ is given by

$$|dd_R\rangle = |dd\rangle + \frac{\mu_{dp}\mu_{df}}{\Delta R^3}|pf\rangle, \tag{6}$$

where states without subscripts are $R=\infty$ states, and Δ is the $dd-pf$ energy detuning shown in Fig. 1.

The linearly polarized microwave electric field $E\cos(\omega t)$ produces the $dd-sf$ coupling,

$$\Omega = \langle dd_R|\frac{\mu E}{2}|sf\rangle = \frac{\mu_{dp}\mu_{df}}{\Delta R^3}\frac{\mu_{ps}E}{2}. \tag{7}$$

The coupling Ω is the Rabi frequency for the transition, and if the product $\Omega T > \pi$, where T is the duration of the microwave pulse, the population oscillates back and forth between the

initially populated dd state and the sf state. The time average probability of being in the sf state is 1/2. The spacing $R = R_T$ is that for which $\Omega T = \pi$. Explicitly,

$$\Omega T = \frac{\mu_{dp}\mu_{df}\mu_{ps}ET}{2\Delta R_T^3} = \pi. \tag{8}$$

For $R < R_T$ we assume the average transition probability to be one-half, and for $R > R_T$ we assume it to vanish, since $\Omega \propto 1/R^3$. For FPT $\ll 1$, $R_T \ll R_{\rm av}$, where $R_{\rm av}$ is related to the local density ρ by

$$\rho = \frac{3}{4\pi R_{\rm av}^3}. \tag{9}$$

In this case,

$$\text{FPT} = \frac{R_T^3}{2R_{\rm av}^3}. \tag{10}$$

From Eqs. (7)–(10) it is evident that

$$\text{FPT} \propto \rho E. \tag{11}$$

That is, FPT is proportional to both density and the microwave field amplitude.

From the six bare states shown in Fgi. 1 we construct six Floquet states which are periodic, with the period of the microwave driving field [13]. The Floquet energies are obtained by adding and subtracting integral multiples of the microwave frequency ω to the bare energies. We are interested in the Forster resonances shown in Fig. 1, which occur when the Floquet states based on the sf, $p_1'f$, $p_3'f$, and $s'f$ states are degenerate with the dd state. For $R = \infty$ and zero microwave field these degeneracies occur when

$$\begin{aligned} W_{sf} - \omega &= W_{dd}, \\ W_{p_1'f} - 2\omega &= W_{dd}, \\ W_{p_3'f} - 2\omega &= W_{dd}, \\ W_{s'f} - 3\omega &= W_{dd}. \end{aligned} \tag{12}$$

Accordingly, we restrict our attention to the Floquet energies W_{dd}, W_{pf}, $W_{sf} - \omega$, $W_{p_1'f} - 2\omega$, $W_{p_3'f} - 2\omega$, and $W_{s'f} - 3\omega$. Ignoring Floquet energies in which other multiples of ω have been added or subtracted is equivalent to making the rotating wave approximation. Figure 2 shows the Floquet energy levels for n=39 as a function of the microwave frequency for vanishing microwave field. The microwave resonances of Fig. 1 correspond to the level crossings of the $42s_{1/2}37f$, $42p_{1/2}37f$, $42p_{3/2}37f$, and $43s_{1/2}37f$ Floquet states with the $39d_{5/2}39d_{5/2}$ state at frequencies 57.878, 55.137, 55.850, and 55.249 GHz. These are the Forster dipole–dipole energy transfer resonances of the dd state with the Floquet states.

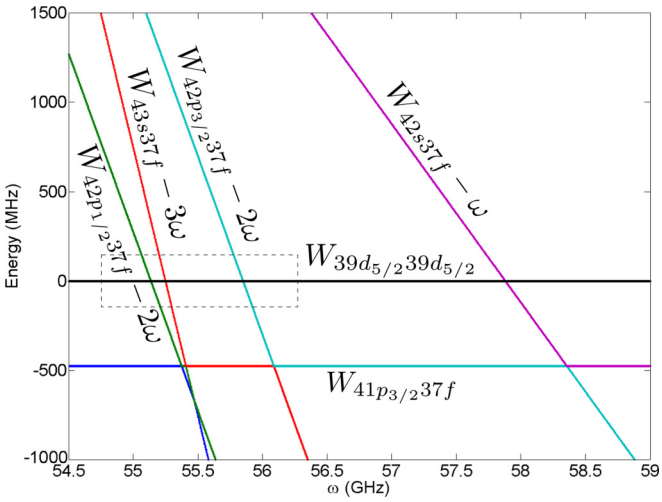

FIG. 2. Floquet energy levels for n=39 as a function of the microwave frequency for zero microwave field amplitude. The energies are specified relative to the energy of the $39d_{5/2}39d_{5/2}$ state.

Equally important are the $42p_{1/2}37f - 43s_{1/2}37f$ and $41p_{3/2}37f - 42s_{1/2}37f$ crossings at 55.473 and 58.356 GHz. These crossings are dipole allowed single photon microwave resonances, and in any finite field they become avoided crossings, altering all the energy levels but that of the $39d_{5/2}39d_{5/2}$ state. These avoided crossings lead to ac Stark shifts of the Forster resonances.

In the presence of the linearly polarized microwave field $E\cos\omega t$ all the levels are coupled, by the matrix elements of Eq. (3), except dd, and the Floquet Hamiltonian matrix can be written as [13]

$$\mathcal{H}_F = \begin{pmatrix} W_{dd} & 0 & 0 & 0 & 0 & 0 \\ 0 & W_{pf} & \mu_{sp}E/2 & 0 & 0 & 0 \\ 0 & \mu_{sp}E/2 & W_{sf}-\omega & \mu_{p_1's}E/2 & \mu_{p_3's}E/2 & 0 \\ 0 & 0 & \mu_{p_1's}E/2 & W_{p_1'f}-2\omega & 0 & \mu_{s'p_1'}E/2 \\ 0 & 0 & \mu_{p_3's}E/2 & 0 & W_{p_3'f}-2\omega & \mu_{s'p_3'}E/2 \\ 0 & 0 & 0 & \mu_{s'p_1'}E/2 & \mu_{s'p_3'}E/2 & W_{s'f}-3\omega \end{pmatrix}. \tag{13}$$

Diagonalizing this matrix yields the eigenvalues and eigenvectors. Since we have ignored the dipole–dipole interaction in this Floquet treatment, the energy W_{dd} does not depend on the microwave field and one of the eigenstates is $|dd\rangle$. Each of the other five eigenstates we label as $|\psi_F\rangle$, where $|\psi_F\rangle$ is the linear combination,

$$|\psi_F\rangle = a_1|pf\rangle + a_2|sf\rangle + a_3|p_1'f\rangle + a_4|p_3'f\rangle + a_5|s'f\rangle. \tag{14}$$

In Fig. 3 we show the Floquet energies over the same frequency range as shown in Fig. 2, but with a microwave field amplitude $E = 415\,\text{mV/cm}$.

The dipole moments of Eq. (13) are matrix elements of z, to correspond to the microwave polarization. We obtained the radial parts from Saffman and Walker [14] and the angular

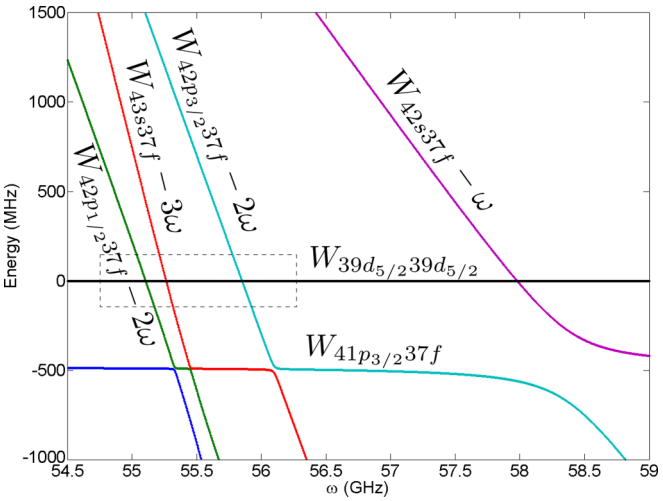

FIG. 3. Floquet energy levels for n=39 as a function of the microwave frequency for microwave field amplitude of 415 mV/cm. The energies are specified relative to the energy of the $39d_{5/2}39d_{5/2}$ state.

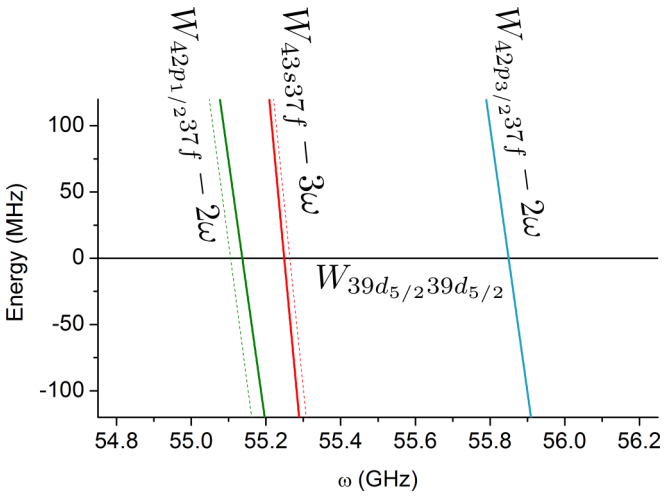

FIG. 4. An expanded view of the region marked by the dashed box in Figs. 2 and 3 containing the two- and three-photon Forster resonances. Solid lines and dotted lines represent microwave coupling of 0 and 200 MHz, respectively. For $W_{42p_{3/2}37f}-2\omega$, the solid line and the dotted line overlap. The energies are specified relative to the energy of the $39d_{5/2}39d_{5/2}$ state.

parts from Edmonds [15]. The specific values used are

$$\begin{aligned}
\mu_{s'p'_3} &= \frac{\sqrt{2}}{3}(1681),\\
\mu_{s'p'_1} &= -\frac{1}{3}(1650),\\
\mu_{p'_1 s} &= -\frac{1}{3}(1752),\\
\mu_{p'_3 s} &= \frac{\sqrt{2}}{3}(1728),\\
\mu_{sp} &= \frac{\sqrt{2}}{3}(1598).
\end{aligned} \tag{15}$$

With the microwave field of 415 mV/cm the matrix element μ_{sp} leads to a microwave coupling of approximately 200 MHz, i.e., $\mu_{sp}E/2 \cong 200$ MHz.

Comparing Fig. 3 to Fig. 2, we can see that the single photon microwave resonances at 55.473 and 58.356 GHz have become obvious avoided crossings, and the two photon $41p_{3/2}37f - 42p_j37f$ resonances are visible. At the single microwave photon resonances the separation between Floquet levels, and the level shifts, are linear in the microwave field. Far from them, for example, at the Forster level crossings with the $39d_{5/2}39d_{5/2}$ state, the level shifts are quadratic in the microwave field. in Fig. 4 we show an expanded view of the portion of Fig. 3 containing the two- and three-photon Forster resonances (marked by dashed boxes in Figs. 2 and 3), in zero field and E=415 mV/cm. At the frequency of the $39d_{5/2}39d_{5/2} - 42p_{3/2}37f$ Forster resonance at 55.850 GHz, the $42p_{3/2}37f$ state lies about halfway between the $43s_{1/2}37f$ and $42s_{1/2}37f$ states, and the ac Stark shifts due to these two states almost cancel, leading to a small ac Stark shift of this Forster resonance. In contrast, at the frequency of the $39d_{5/2}39d_{5/2} - 42p_{1/2}37f$ Forster resonance at 55.137 GHz, the $42p_{1/2}37f$ state is below both the $42s_{1/2}37f$ and $43s_{1/2}37f$ states, so the ac Stark shifts add. More important, the Forster resonance is very close to the single-photon $42p_{1/2}37f - 43s_{1/2}37f$ resonance, leading to a large frequency shift.

For small microwave fields the ac Stark shifts of the Forster resonances are quadratic in the microwave field amplitude, and the calculated ac Stark shifts are presented with the experimental results in the next section.

To calculate the fractional population transfer (FPT) from the laser excited dd state to a Floquet state at a Forster resonance, we follow a procedure similar to that used in the development of Eqs. (7)–(10). We compute the transition probability for a pair of atoms spaced by distance R and then average over the distribution of the spacings in the trap volume.

We calculate the transition probability at resonance for a transition from the dd state to the Floquet state for a pair as follows. The microwave field is switched on and off in 10 ns, which is fast compared to the dipole–dipole interaction. Thus, when the microwave field is switched on the population oscillates between $|dd\rangle$ and $|\psi_F\rangle$ at the frequency Ω given by the dipole–dipole coupling matrix element $\Omega = \langle dd|\frac{\mu\mu'}{R^3}|\psi_F\rangle$. Since only the $|pf\rangle$ part of the $|\psi_F\rangle$ eigenfunction contributes to this matrix element,

$$\Omega = \langle dd|\frac{\mu\mu'}{R^3}|\psi_F\rangle = a_1\langle dd|\frac{\mu\mu'}{R^3}|pf\rangle, \tag{16}$$

where a_1 is the coefficient given in Eq. (14). For $\Omega T > \pi$, on average half the oscillating population is in the ψ_F state and is left there when the microwave field is turned off, in 10 ns. As in the earlier development of Eqs. (7)–(10),the condition $\Omega T = \pi$ is met for $R = R_T$ where

$$\Omega T = a_1\langle dd|\frac{\mu\mu'}{R_T^3}|pf\rangle T = \pi. \tag{17}$$

For $R < R_T$, $\Omega T > \pi$, and the average transition probability is one-half. For $R > R_T$ the transition probability falls rapidly with R. Accordingly, pairs with $R < R_T$ undergo the

TABLE I. Microwave field amplitudes required to produce $a_1 = 0.05$ for $n = 39$.

Transition	Required microwave field amplitude (mV/cm)
$nd_{5/2}nd_{5/2} \rightarrow (n+3)s_{1/2}(n-2)f_{7/2}$	49.8
$nd_{5/2}nd_{5/2} \rightarrow (n+3)p_{1/2}(n-2)f_{7/2}$	622.5
$nd_{5/2}nd_{5/2} \rightarrow (n+3)p_{3/2}(n-2)f_{7/2}$	456.5
$nd_{5/2}nd_{5/2} \rightarrow (n+4)s_{1/2}(n-2)f_{7/2}$	1369.5

transition, and the FPT is again

$$\mathrm{FPT} = \frac{R_T^3}{2R_{av}^3}. \tag{18}$$

The population oscillation frequency Ω and the FPT are proportional to the Rydberg atom density and a_1, the coefficient of the pf component of ψ_F. In the low microwave field limit, at each of the Forster resonances a_1 is proportional to E^M, where M is the number of the photons absorbed or emitted.

To verify that the Floquet model gives the same result as the CI model discussed earlier, we restrict our attention to the one-photon case treated using the CI model. For the one-photon $dd - sf$ Forster resonance the microwave power is sufficiently low that only three states need to be considered, dd, pf, and sf. In this case the only coupling in the Floquet matrix of Eq. (13) is that between the pf and sf states, and

$$a_1 = \frac{\mu_{ps}E}{2(W_{sf} - \omega - W_{pf})}. \tag{19}$$

Since, at resonance $W_{sf} - \omega = W_{dd}$ [see Eq. (12)], we can write the oscillation frequency Ω as

$$\Omega = \frac{\mu_{ps}\mu_{dp}\mu_{df}E}{2\Delta R^3}, \tag{20}$$

which is precisely the CI result of Eq. (7). In sum, the Floquet model allows us to predict the ac Stark shifts of the multiphoton resonances and the fractional population transfers, which scale as E^M, where M is the number of microwave photons emitted or absorbed. Furthermore, the Floquet description is equivalent to the CI model presented previously to describe one-photon transitions.

To compute the microwave fields required to observe the different transitions shown in Fig. 1, a useful criterion is the field required to produce a fixed value of a_1. In Table I we give the microwave fields required to produce $a_1 = 0.05$ for n=39. For the two-photon transitions of Fig. 1 this criterion requires $E \approx 550$ mV/cm, comparable to the microwave field amplitude of 415 mV/cm that was used to generate Fig. 3. From Table I it is apparent that similar microwave field strengths are required to observe the two-photon transitions $dd \rightarrow p_1' f$ and $dd \rightarrow p_3' f$, since the detuning from the intermediate sf state is large in both cases. However, the ac Stark shift of the $dd \rightarrow p_1' f$ resonance is much larger due to the proximity of the $dd \rightarrow p_1' f$ Forster resonance to the single microwave photon $p_1' f \rightarrow s' f$ resonance.

III. EXPERIMENTAL APPROACH

The essential notion of the experiment can be understood with the aid of Fig. 5, which shows the relevant energy levels of single microwave photon transitions from the $nd_{5/2}nd_{5/2}$ state. Pulsed 480-nm laser excitation of atoms to the $nd_{5/2}$ state produces $nd_{5/2}nd_{5/2}$ pairs, which are coupled by the dipole–dipole interaction to the energetically nearby $(n+2)p_{3/2}(n-2)f$ state. A 1-μs-long microwave pulse drives one of the four transitions, labeled A–D, in Fig. 5. In CI terms, the transitions are allowed due to the admixture of the $(n+2)p_{3/2}(n-2)f$ state into the $nd_{5/2}nd_{5/2}$ state by the dipole–dipole interaction. One of the atoms in the admixture interacts with the microwave field while the other remains a spectator. As shown by fig. 5, which is approximately to scale, the microwave field can drive the pair to a lower or higher energy state. We detect that the pair has undergone the transition by applying a field ionization pulse after the microwave pulse. We assume that the field ionization pulse projects the atoms onto isolated atomic states. For a transition to be observable one of the atoms in the final state pair must have an energy above the energy of the initially

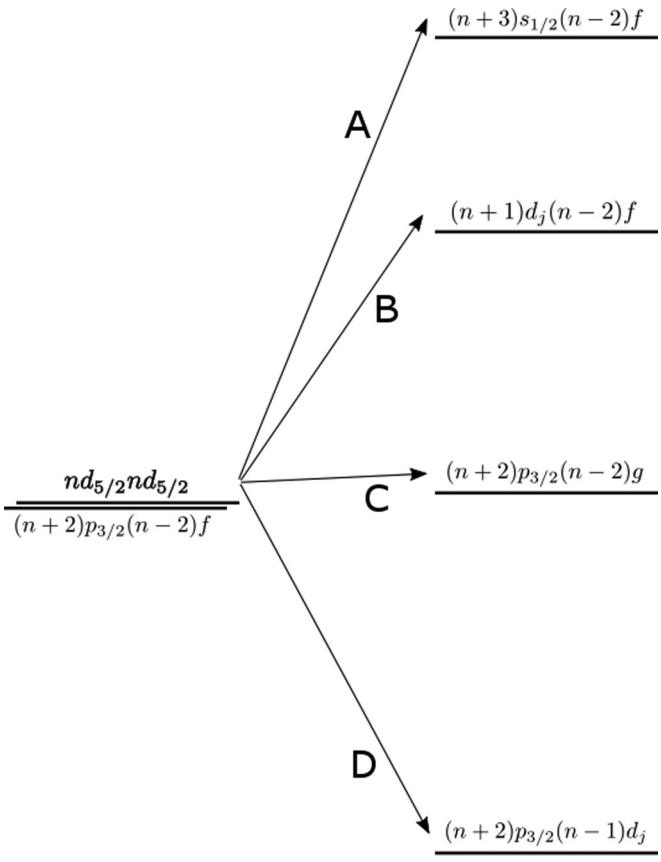

FIG. 5. The observed one-photon transitions originating from $nd_{5/2}nd_{5/2}$. The $(n+2)p_{3/2}(n-2)f$ state is nearly degenerate with the $nd_{5/2}nd_{5/2}$ level. For $n = 39$, the $(n+2)p_{3/2}(n-2)f$ level is detuned by 477.8 MHz.

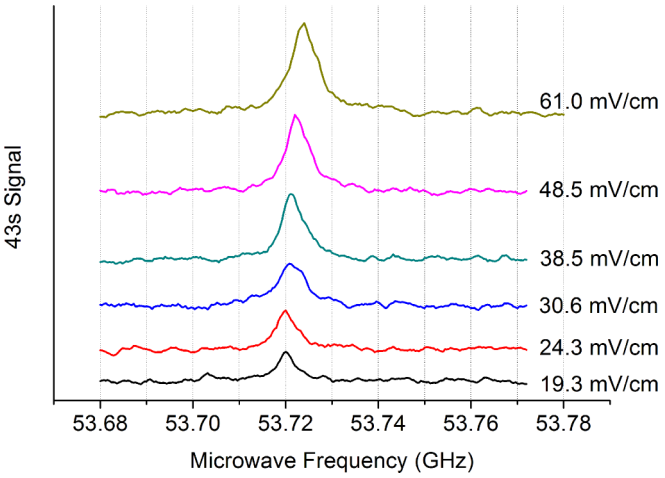

FIG. 6. Observed $40d_{5/2}40d_{5/2} \rightarrow 43s_{1/2}38f_{7/2}$ resonances for a range of microwave field amplitudes. The calculated resonance frequency for the transition at zero microwave power and $R = \infty$ is 53.721 GHz.

excited nd state so that it is ionized earlier in the field ionization pulse. The $(n+2)p_{3/2}$, $(n+1)d_j$, and $(n+3)s_{1/2}$ states meet this criterion. It is useful to note that in transition D although the microwave transition removes energy from the pair, the transition is detectable since the result is an $(n+2)p_{3/2}$ atom, which lies above the $nd_{5/2}$ state. The resonances corresponding to the transitions shown in Fig. 5 are recorded by setting the gate of a gated integrator on the signal due to field ionization of the $(n+2)p_{3/2}$, $(n+1)d_j$, or $(n+3)s_{1/2}$ state and slowly sweeping the microwave frequency over many shots of the laser.

Since this experiment is an extension of work reported previously [5], the experimental approach has much in common. ^{85}Rb atoms are trapped in a vapor loaded magneto-optical trap (MOT), which supplies a steady population of Rb atoms in the $5p_{3/2}$ state. Atoms are excited to the $nd_{5/2}$ or $ns_{1/2}$ state by a 10-μJ 480-nm laser pulse which is generated by pulse amplifying, at a 20-Hz repetition rate, and then frequency doubling the output of tapered amplifier seeded by a 960-nm single mode diode laser. The 480-nm pulse is 10-ns long and has a bandwidth of 150 MHz. Approximately 4 ms before the excitation with the pulsed laser, the trap magnetic fields are switched off so that the residual field at the center of MOT during the experiment is reduced to less than 50 mG. Subsequent to laser excitation, the atoms are exposed to a 1-μs-long microwave pulse to drive the transitions shown in Fig. 5; 65 ns after the end of the microwave pulse, a 3-μs rise time field ionization pulse is applied to field ionize the Rydberg atoms and drive the resulting ions to a microchannel plate (MCP) detector. The signal from the MCP is recorded with a gated integrator and stored in a computer for later analysis.

The cloud of cold Rb atoms is held at the center of four stainless steel vertical rods which pass through the corners of a horizontal square 18 mm on a side. The positive field ionization voltage pulse is applied to the rods farther from the MCP while the two rods closer to the MCP are grounded. The density of Rydberg atoms in the MOT is determined in the following way. The 780-nm fluorescence from the MOT is measured to find the total number of the trapped atoms in the $5p_{3/2}$ state. Then, the number of Rydberg atoms excited on each laser shot can be determined by combining the measured reduction of the $5p_{3/2}$ population when the pulsed Rydberg excitation is added and the 1-s filling time of the trap. The density of the Rydberg atoms is determined by measuring the waist of the 480-nm beam and the diameter of the MOT. It is assumed that the Rydberg atom density has the following form: $\rho(x,y,z) = \rho_0 e^{-(x^2+y^2+z^2)/r_M^2} e^{-(x^2+y^2)/r_L^2}$, where $r_M = 0.5$ mm and $r_L = 0.18$ mm are the radii of the MOT and the 480-nm laser beam, respectively; ρ_0 is the density at the center of the trap; and x, y, and z are the Cartesian displacements from the center of the trap. The 480-nm beam propagates in the z direction. In these experiments, the maximum value of ρ_0 is $5 \times 10^8 \mathrm{cm}^{-3}$, and the density measurement uncertainty is a factor of three.

The microwaves are generated in an Agilent E8247C synthesizer, which has a maximum frequency of 20 GHz, and a General Microwave DM862B switch is used to form the microwaves into 1-μs-long pulses. A Narda DBS2640X220 active doubler and a DBS4060X410 active quadrupler are used to generate microwaves in the 26.5–40 GHz and 40–60 GHz ranges, respectively. The relative microwave power is controlled in the final waveguide with a HP R832A or U832A precision attenuator. The microwaves have horizontal polarization and propagate from a horn outside the vacuum

TABLE II. Resonance frequencies and ac Stark shifts for one-photon transitions. Calculated shifts are obtained from our Floquet model. The estimated maximum field amplitudes are calculated from the maximum observed shifts and calculated shifts.

Transition	n	Calculated (GHz)	Observed (GHz)	Calculated Shift [MHz/(V/cm)^2]	Max. Observed Shift (MHz)	Estimated Max. Field Amplitude (mV/cm)
$nd_{5/2}nd_{5/2} \rightarrow (n+3)s_{1/2}(n-2)f_{7/2}$	39	57.878	57.876(9)	486.8	18.4	194
	40	53.721	53.719(11)	791.1	73.4	305
$nd_{5/2}nd_{5/2} \rightarrow (n+2)p_{3/2}(n-1)d_{5/2}$	39	43.921	43.923(8)	348.4	29.4	290
	40	40.415	40.417(8)	570.6	20.1	188
$nd_{5/2}nd_{5/2} \rightarrow (n+2)p_{3/2}(n-1)d_{3/2}$	39	44.138	44.139(3)	455.3	12.8	168
	40	40.615	40.616(6)	745.7	10.7	120
$nd_{5/2}nd_{5/2} \rightarrow (n+2)p_{3/2}(n-2)g$	41	1.190	1.190(11)	130.9	3.3	159
	42	1.194	1.190(5)	305.2	3.6	109
$ns_{1/2}ns_{1/2} \rightarrow (n-1)d_{5/2}(n-1)p_{3/2}$	39	34.010	34.010(9)	36.7	<1	
	40	31.441	31.441(10)	44.9	<1	

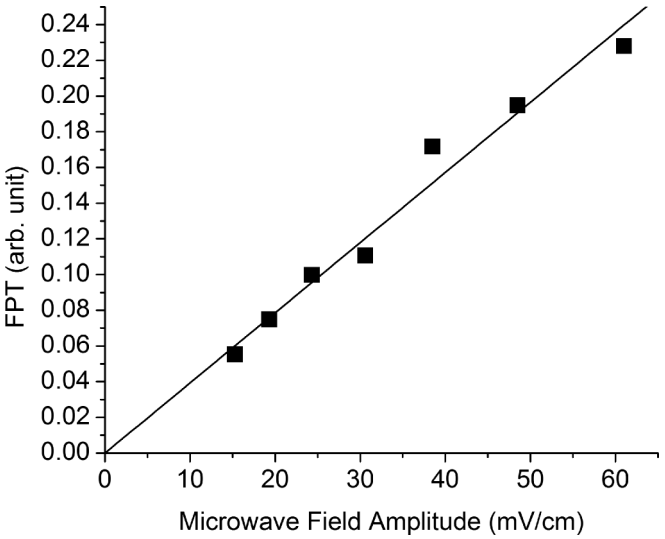

FIG. 7. Fractional population transfer (FPT) vs microwave field amplitude for the $40d_{5/2}40d_{5/2} \rightarrow 43s_{1/2}38f_{7/2}$ transition.

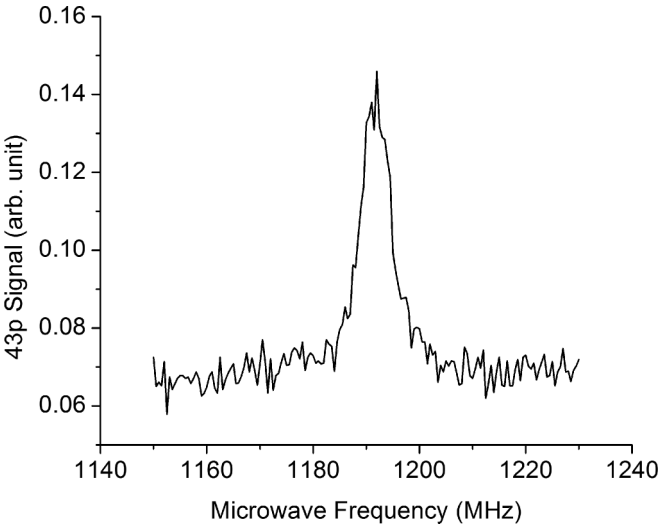

FIG. 8. Observed resonance for the $41d_{5/2}41d_{5/2} \rightarrow 43p_{3/2}39g$ transition. The peak is shifted to higher frequency by 1.4 MHz due to ac Stark shift. The calculated frequency for the transition is 1190.4 MHz.

system through a window to the MOT volume. The vertical rods used to apply field ionization pulse scatter the microwaves to some extent, and this results in the polarization's not being perfectly linear. Some of the transitions require low frequencies, in the vicinity of 1 GHz. For those transitions, the output of the Agilent E8247C synthesizer is directly connected to the pair of rods closest to the MCP after going through a Mini-circuits ZHL-42W amplifier and an E&M Labs L30Y circulator. In most cases, there is an ac Stark shift due to near resonance of the microwaves to some other transition. Since the state that is responsible for the ac Stark shift is different for each transition, more detail will be provided when discussing each transition. It is straightforward to extrapolate the location of the resonance peaks to zero microwave power, and the power shift is used to estimate the absolute microwave field amplitude over the range of frequencies employed.

IV. OBSERVATIONS

A. One-photon transitions from $nd_{5/2}nd_{5/2}$

In Fig. 5 we show the single-photon transitions from the $nd_{5/2}nd_{5/2}$ state. In all cases these transitions are possible due to the dipole–dipole induced admixture of the nearly degenerate $(n+2)p_{3/2}(n-2)f$ state into the $nd_{5/2}nd_{5/2}$ state.

1. $nd_{5/2}nd_{5/2} \rightarrow (n+3)s_{1/2}(n-2)f$, Transition (A)

Figure 6 shows the observed $40d_{5/2}40d_{5/2} \rightarrow 43s_{1/2}38f_{7/2}$ resonances for a range of microwave field amplitudes. This transition corresponds to the transition A in Fig. 5 when $n = 40$. As the microwave field amplitude is raised, the transition exhibits an ac Stark shift to higher frequency. The ac Stark shift is caused by the fact that this transition is nearly resonant with the atomic $42p_{3/2} \rightarrow 43s_{1/2}$ transition. The relative microwave fields are determined from attenuator settings, whereas the absolute fields given in Fig. 6 are determined by calculating how much field is required to produce the observed shifts. In Table II we also present the ac Stark shifts calculated from our Floquet model as well as the maximum ac Stark shifts observed and the estimated maximum field amplitude. Although we have not made careful measurements of the microwave field amplitudes, they are consistent with the maximum field ~0.7 V/cm we expect for our microwave system, which has a maximum power of 100 mW and a horn with a gain of 20 dB located 20 cm from the trapped atoms. The resonance frequency at zero microwave power is obtained by extrapolating the frequency of the resonance peak at different microwave field amplitudes back to zero power. The zero microwave power frequencies for our measurements are summarized in Table II. Based on

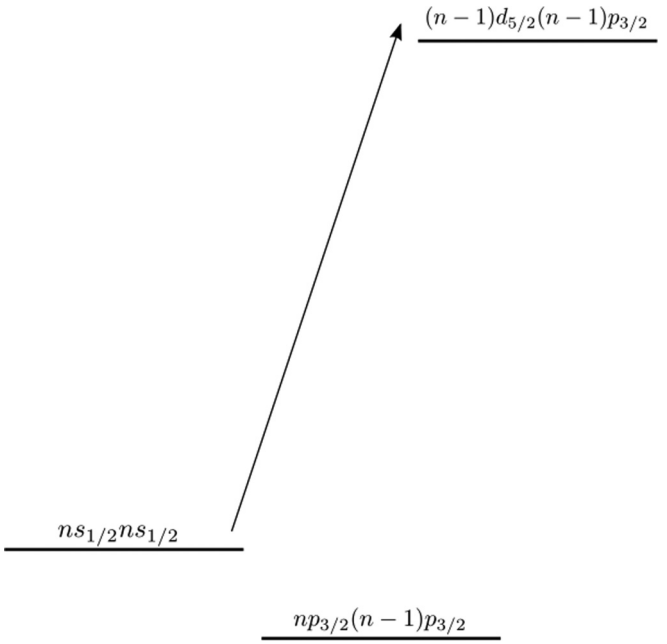

FIG. 9. Energy levels for the one-photon transition $ns_{1/2}ns_{1/2} \rightarrow (n-1)d_{5/2}(n-1)p_{3/2}$.

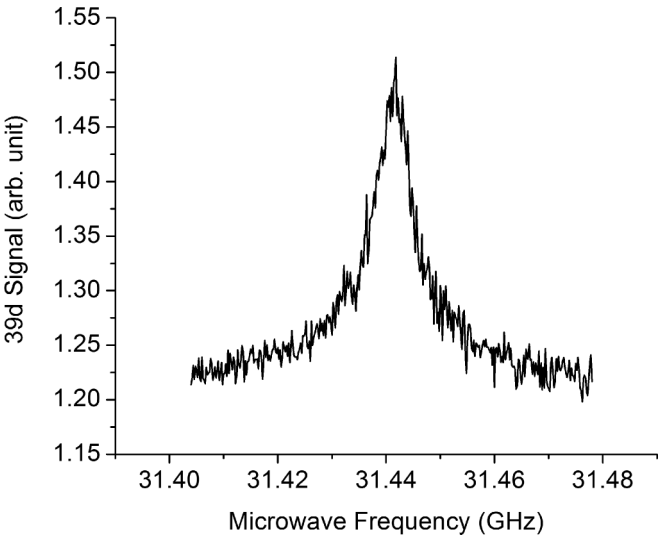

FIG. 10. Observed resonance for the $40s_{1/2}40s_{1/2} \rightarrow 39d_{5/2}39p_{3/2}$ transition. The calculated frequency for the transition is 31.441 GHz. The peak is not observably shifted.

either the CI or Floquet model for a single-photon transition, the fraction of atoms that is transferred to $(n+3)s_{1/2}(n-2)f$ state is expected to depend linearly on the microwave field amplitude. Figure 7 shows the plot of FPT vs the microwave field amplitude, exhibiting the expected linear behavior.

2. $nd_{5/2}nd_{5/2} \rightarrow (n+1)d_j(n-2)f$, *Transition (B)*

Transition B in Fig. 5 was first reported by Yu *et al.* [6] in 2013. Further investigation of transition B as well as the observation of transition D were reported in the previous paper [5].

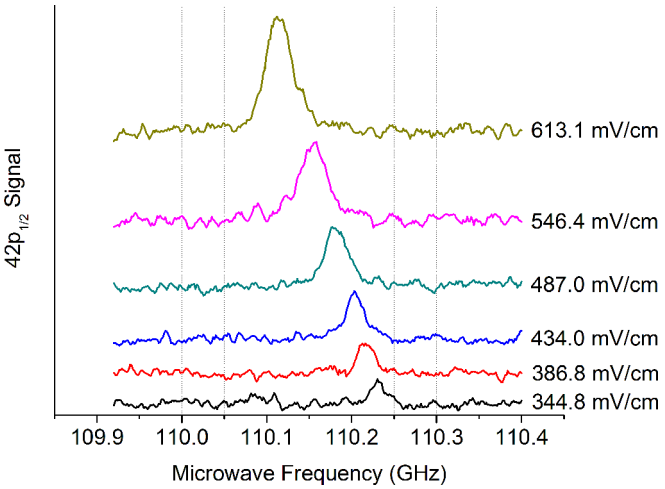

FIG. 11. Observed $39d_{5/2}39d_{5/2} \rightarrow 42p_{1/2}37f$ resonances for a range of microwave field amplitudes. The calculated resonance frequency for the transition at zero microwave power and $R = \infty$ is 110.273 GHz.

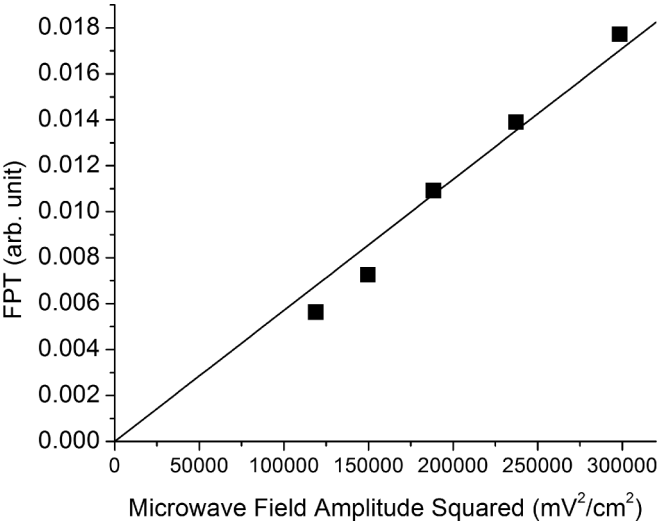

FIG. 12. Fractional population transfer (FPT) vs microwave field amplitude squared for the $39d_{5/2}39d_{5/2} \rightarrow 42p_{1/2}37f$ transition.

3. $nd_{5/2}nd_{5/2} \rightarrow (n+2)p_{3/2}(n-2)g$, *Transition (C)*

Unlike transitions A and B of Fig. 5, in this case it is the $(n-2)f$ atom which undergoes the transition. Figure 8 shows the resonant peak for the $41d_{5/2}41d_{5/2} \rightarrow 43p_{3/2}39g$ transition, which corresponds to transition C in Fig. 5. Due to the low frequency range required for the transition, the output of the microwave synthesizer is connected directly to the pair of rods closest to the MCP, as mentioned in the previous section. The transitions exhibit an ac Stark shift, linear in the radio frequency power, of up to 3 MHz, and the resonance frequencies at zero power are obtained by extrapolating to zero power. The results are summarized in Table II. The ng-series quantum defect that is needed to calculate the intervals was taken from the paper by Lee *et al.* [12].

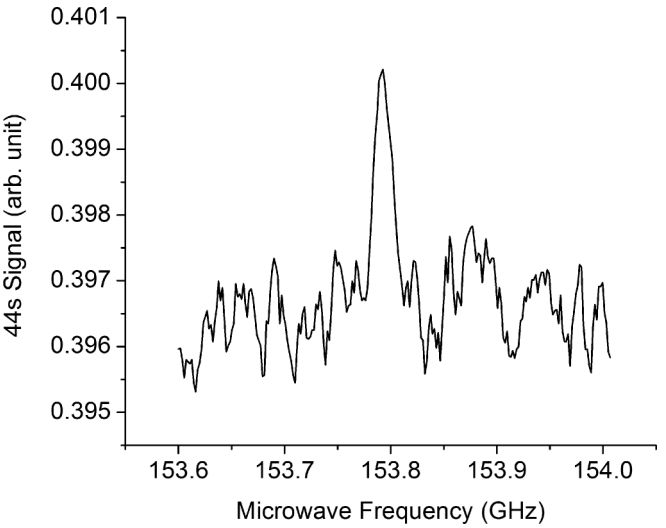

FIG. 13. The observed resonance for the $40d_{5/2}40d_{5/2} \rightarrow 44s_{1/2}38f$ transition. The peak is shifted to higher frequency by 25 MHz due to ac Stark shift.

TABLE III. Resonance frequencies and ac Stark shifts for two-photon transitions. Calculated shifts are obtained from our Floquet model. The estimated maximum field amplitudes are calculated from the maximum observed shifts and calculated shifts.

Transition	n	Calculated (GHz)	Observed (GHz)	Calculated Shift [MHz/(V/cm)^2]	Max. Observed Shift (MHz)	Estimated Max. Field Amplitude (mV/cm)
$nd_{5/2}nd_{5/2} \rightarrow (n+3)p_{1/2}(n-2)f_{7/2}$	39	110.273	110.280(51)	419.9	118.6	531
	40	102.294	102.294(31)	482.1	50.8	325
$nd_{5/2}nd_{5/2} \rightarrow (n+3)p_{3/2}(n-2)f_{7/2}$	39	111.699	111.697(18)	8.6	<1	
	40	103.617	103.615(10)	15.5	<1	

4. $nd_{5/2}nd_{5/2} \rightarrow (n+2)p_{3/2}(n-1)d_{5/2}$, Transition (D)

There are two notable aspects to this transition. In addition to the $(n-2)f$ atom undergoing the transition, the transition is to a molecular state lower in energy than the $nd_{5/2}nd_{5/2}$ state. However, the atom left in the $(n+2)p_{3/2}$ state gains energy and can be distinguished from an $nd_{5/2}$ atom by field ionization. The observation of this transition was first reported in the previous paper [5]. In Table II, we report more systematic measurements made to determine the transition frequencies at zero microwave power.

B. One-photon transitions from $ns_{1/2}ns_{1/2}$

For the transitions originating from the $nd_{5/2}nd_{5/2}$ state, it is the dipole–dipole induced configuration interaction with the nearby $(n+2)p_{3/2}(n-2)f$ state that allows the transitions. If we start with the $ns_{1/2}ns_{1/2}$ state, the nearest dipole–dipole coupled state, $np_{3/2}(n-1)p_{3/2}$, is much further away. As a concrete example, for $n=40, \Delta_{40s_{1/2}40s_{1/2}-40p_{3/2}39p_{3/2}} = 5.45\,\text{GHz}$, whereas $\Delta_{40d_{5/2}40d_{5/2}-42p_{3/2}38f_{7/2}} = 325\,\text{MHz}$. The large detuning for $ns_{1/2}ns_{1/2} - np_{3/2}(n-1)p_{3/2}$ results in a small admixture coefficient. Nonetheless, it is possible to observe transitions similar to the observed transitions originating from the $nd_{5/2}nd_{5/2}$ state.

$ns_{1/2}ns_{1/2} \rightarrow (n-1)d_{5/2}(n-1)p_{3/2}$

Figure 9 shows the energy levels involved in the $ns_{1/2}ns_{1/2} \rightarrow (n-1)d_{5/2}(n-1)p_{3/2}$ transition which is one of the possible transitions originating from the $ns_{1/2}ns_{1/2}$ state. The diagram is approximately to scale, and the large detuning between $ns_{1/2}ns_{1/2}$ and $np_{3/2}(n-1)p_{3/2}$ is evident. Figure 10 shows the observed resonance for $n=40$. The resonant peak does not observably shift when the microwave power is raised because the microwave frequency is not near the $40p_{3/2} \rightarrow 39d_{5/2}$ resonant frequency.

C. Multiphoton transitions from $nd_{5/2}nd_{5/2}$

In addition to the transitions discussed so far, transitions that involve more than one microwave photon have been observed. Figure 1 shows the observed single- and multiphoton transitions originating from the $nd_{5/2}nd_{5/2}$ state. Observing the multiphoton transitions requires higher microwave field amplitude.

1. $nd_{5/2}nd_{5/2} \rightarrow (n+3)p_{1/2}(n-2)f$

Figure 11 shows the observed $39d_{5/2}39d_{5/2} \rightarrow 42p_{1/2}37f$ resonances for a range of microwave field amplitudes. This is a two-photon transition, and the resonances exhibit a large ac Stark shift to lower frequency. The microwave field amplitudes involved here are greater than those in Fig. 6 by more than an order of magnitude. The microwave field amplitudes were estimated from the observed shifts. As discussed earlier, for a two-photon transition, the fraction of atoms that is transferred to the $(n+3)p_j(n-2)f$ state is expected to scale as the square of the microwave field amplitude, or linearly in the microwave power. Figure 12 shows the plot of FPT vs microwave field amplitude squared, which is linear, as expected. The obtained zero power frequencies are given in Table III.

2. $nd_{5/2}nd_{5/2} \rightarrow (n+3)p_{3/2}(n-2)f$

Although the frequency for this transition lies near the $nd_{5/2}nd_{5/2} \rightarrow (n+3)p_{1/2}(n-2)f$ transition frequency, there is an important difference: The resonant peak for this transition does not observably shift when the microwave power is raised. As discussed earlier, the suppression of the ac Stark shift is caused by the fact that the $(n+3)p_{3/2}$ state lies approximately halfway between the $(n+3)s_{1/2}$ and $(n+4)s_{1/2}$ states. As a result, the ac Stark shift contributions due to the $(n+3)s_{1/2}$ and $(n+4)s_{1/2}$ states nearly cancel. The calculated ac Stark shifts are given in Table III as well as the observed and calculated zero power frequencies.

3. $nd_{5/2}nd_{5/2} \rightarrow (n+4)s_{1/2}(n-2)f$

Figure 13 shows the observed resonance for the $40d_{5/2}40d_{5/2} \rightarrow 44s_{1/2}38f$ transition. The peak is shifted to higher frequency by 25 MHz by the ac Stark shift. This three-photon transition requires a high microwave field amplitude, and the resonance peaks can only be obtained for the microwave field amplitudes close to the maximum possible

TABLE IV. Resonance frequency and ac Stark shift for the three-photon transition. The calculated shift is obtained from our Floquet model. The estimated maximum field amplitude is calculated from the maximum observed shift and calculated shift.

Transition	n	Calculated (GHz)	Observed (GHz)	Calculated Shift [MHz/(V/cm)^2]	Max. Observed Shift (MHz)	Estimated Max. Field Amplitude (mV/cm)
$nd_{5/2}nd_{5/2} \rightarrow (n+4)s_{1/2}(n-2)f_{7/2}$	40	153.768	153.767(79)	87.2	40.2	679

value. The calculated ac Stark shifts are given in Table IV as well as the observed and calculated zero power frequencies.

V. CONCLUSION

These measurements show that it is straightforward to drive microwave transitions between pairs of atoms even when the dipole-dipole detuning is large, ∼5 GHz. Both single photon and multiphoton transitions can be described as Forster resonances of Floquet states tuned into resonance with the microwave frequency. The Floquet approach is particularly convenient for multiphoton transitions as it is easily extended to stronger fields, and it reduces to the CI approach used previously for single-photon transitions.

ACKNOWLEDGMENTS

We acknowledge useful comments from R. R. Jones. This work has been supported by the Air Force Office of Scientific Research under Grant No. FA9550-14-1-0288. J.I. would like to thank the Higher Education Commission of Pakistan for support.

[1] R. C. Teixeira, C. Hermann-Avigliano, T. L. Nguyen, T. Cantat-Moltrecht, J. M. Raimond, S. Haroche, S. Gleyzes, and M. Brune, Phys. Rev. Lett. **115**, 013001 (2015).
[2] C. S. E. van Ditzhuijzen, A. F. Koenderink, J. V. Hernández, F. Robicheaux, L. D. Noordam, and H. B. van L. van den Heuvell, Phys. Rev. Lett. **100**, 243201 (2008).
[3] P. Pillet, R. Kachru, N. H. Tran, W. W. Smith, and T. F. Gallagher, Phys. Rev. A **36**, 1132 (1987).
[4] H. Park, T. F. Gallagher, and P. Pillet, Phys. Rev. A **93**, 052501 (2016).
[5] J. Lee and T. F. Gallagher, Phys. Rev. A **93**, 062509 (2016).
[6] Y. Yu, H. Park, and T. F. Gallagher, Phys. Rev. Lett. **111**, 173001 (2013).
[7] H. Saßmannshausen, F. Merkt, and J. Deiglmayr, Phys. Rev. A **92**, 032505 (2015).
[8] W. E. Cooke, T. F. Gallagher, S. A. Edelstein, and R. M. Hill, Phys. Rev. Lett. **40**, 178 (1978).
[9] N. H. Tran, P. Pillet, R. Kachru, and T. F. Gallagher, Phys. Rev. A **29**, 2640 (1984).
[10] W. Li, I. Mourachko, M. W. Noel, and T. F. Gallagher, Phys. Rev. A **67**, 052502 (2003).
[11] J. Han, Y. Jamil, D. V. L. Norum, P. J. Tanner, and T. F. Gallagher, Phys. Rev. A **74**, 054502 (2006).
[12] J. Lee, J. Nunkaew, and T. F. Gallagher, Phys. Rev. A **94**, 022505 (2016).
[13] J. H. Shirley, Phys. Rev. **138**, B979 (1965).
[14] T. G. Walker and M. Saffman, Phys. Rev. A **77**, 032723 (2008).
[15] A. Edmonds, *Angular Momentum in Quantum Mechanics* (Princeton University Press, Princeton, 1960).